Chapter 2

Theoretical Part

2.1 Glass formation

2.1.1 Definition of glass

The definition from 1945 of the American society for testing and materials could be mentioned. " Glass is an inorganic product of fusion which has been cooled to a rigid condition without crystallizing." The physicochemical of glass is a special interest that can be explained as a process of glass production and to observation the behavior of a particular property. In Figure 2-1, at high temperature where a glass melts, the volume of the liquid glass here should be investigated. When a liquid or a melt cools, its volume will decrease. Generally, crystal occurs at the melting point (T_m), whereby a decrease in volume ensures. As the temperature is lower, the crystal volume will be decreased further. Therefore, when no crystal occurs at T_m, then the volume must be decreased continuously along the dashed equilibrium curve, which this area is so-called supercooled melt or can be referred that liquid is still in a metastable state or thermodynamic equilibrium. At the liquid has become a solid and the equilibrium is no longer possible, is so-called the transformation/transition temperature (T_g). Simon[2] called this phenomenon the freezing-in process. And we can define:

"In the physicochemical sense, glass is a frozen-in undercooled liquid."

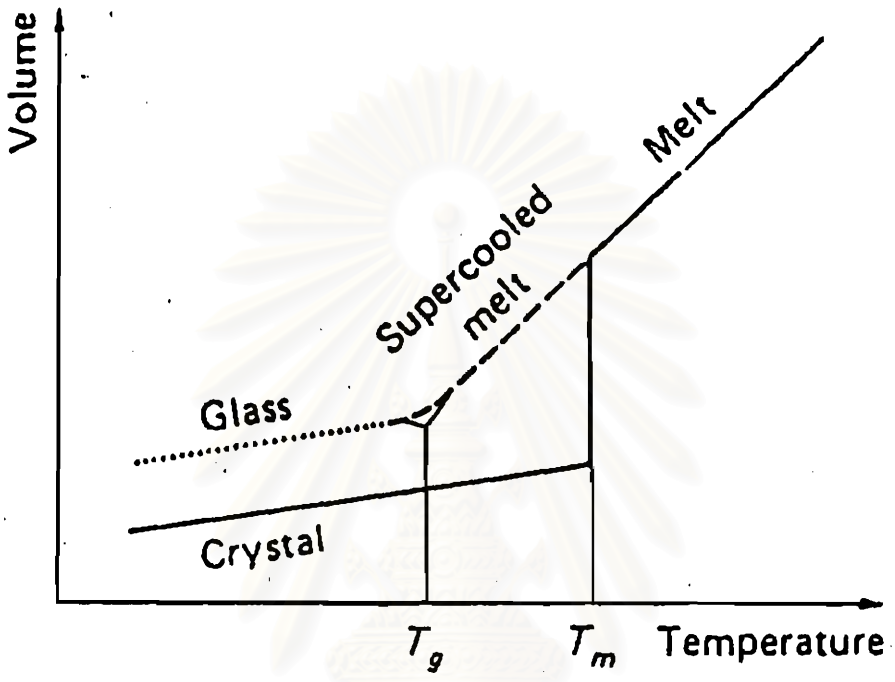

Figure 2-1 Schematic diagram of the temperature dependence of volume.[3]

2.1.2 Approaches to glass formation[4]

A variety of approaches of glass formation can be categorized as:

1. Structural approaches

This approaches explain whether structures are conductive to ease of glass formation but do not directly address the glass formation. The best known of these approaches is based on the random network model.

2. Thermodynamic approaches

Energetic distinctions between network-forming and network-modifying cations in oxide system have been made on several bases, e.g. field strength, single bond strength, and electronegativity will be described, but they leave unaddressed the contributions of different network-forming or network-modifying cations to the ease or difficulty of forming glass.

3. Kinetic approaches

Two above approaches are concerned with identifying the structural or thermodynamic factors which determine whether a material will form a glass when cooled from the liquid state. In contrast, the kinetic approaches are concerned with how fast must a given material be cooled so that defectable crystallization can be avoided.

2.1.3 Kinetic treatment of glass formation

The volume fraction crystallized V_c/V in time t can be expressed

$$V_c/V = 1 - \exp\left[-\int_0^t I_v \left(\int_t^{t'} U d\tau\right)^3 dt'\right] \qquad (2\text{-}1)$$

where I_v - the nucleation rate per unit volume

U - the crystal growth rate.

When cooling, both I_v and U are time-dependent through their dependence on temperature. For isothermal crystallization, I_v and U are constant, this reduces to

$$V_c / V = 1 - \exp\left[-\frac{\pi}{3} I_v U^3 t^4\right]. \qquad (2\text{-}2)$$

If I_v and U are known at a given temperature, the time requires to reach the critical V_c/V can be calculated from Equations 2-1 and 2-2. By repeating such calculations for different temperatures, the locus of times required to reach the particular fraction crystallized can be represented in a familiar time-temperature-transformation (TTT) diagram. This is illustrated in Figure 2-2.

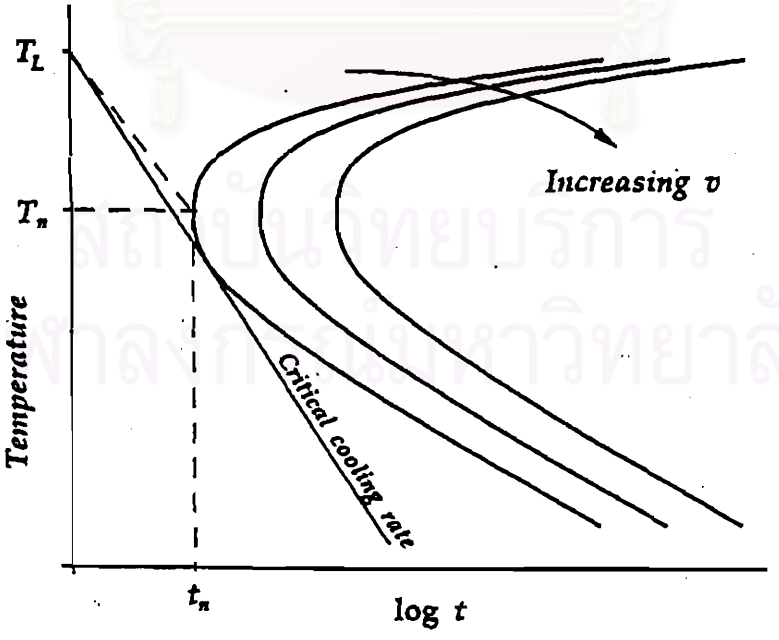

Figure 2-2 Time-temperature-transformation (TTT) curve.[5]

Each TTT curve has an extremum or nose, which reflects a competition between the driving force for crystallization and the molecular mobility and represents the least time required to form the given fraction crystallized.

The critical cooling rate R_c, required to avoid a given fraction crystallized can be obtained by the "nose method" which is estimated as:

$$R_c \approx \frac{T_m - T_n}{t_n} \qquad (2\text{-}3)$$

when T_m - melting or liquidus temperature

T_n, t_n - temperature and time of the nose at the TTT curve.

Most evaluation of the critical cooling rates for glass formation take I_v and in the range of high undercoolings near the noses of TTT curves, homogeneous nucleation represents the dominant contribution to the formation of crystal nuclei. However, it is recognized that consideration of homogeneous nucleation directs attention to the minimum cooling rates required to form glasses.

Otherwise, the effects of heterogeneous nuclei on the critical cooling rates required to form glasses. Using the analysis of crystallization statistics, it was found that heterogeneities with contact angle (θ) greater than about 100° should have no effect on the critical cooling rates for glass formation. For smaller contact angles, the critical cooling rate should increase with decreasing. This is illustrated in Figure 2-3.

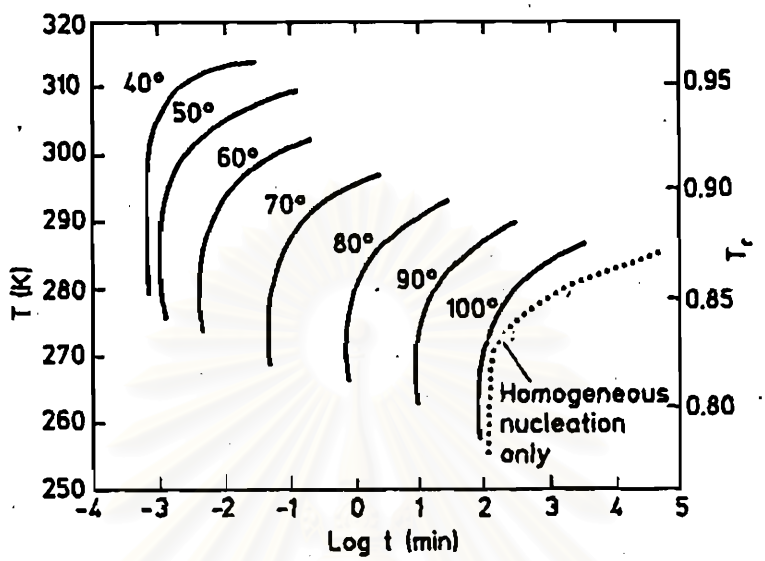

Figure 2-3 Continuous cooling curves for homogeneous nucleation + bulk heterogeneous nucleation for 0 - terphenyl containing to 10^{7} heterogeneities cm^{-3} having contact angles indicated.[6]

2.1.4 Material characteristics and glass formation[4]

Material characteristics, which are conducive to glass formation, must lead to reduce the critical cooling rate as following:

1. A high viscosity at the temperature of the nose of the TTT curve. At this temperature of fastest overall crystallization rate, a high viscosity implies a low crystallization rate and hence a low critical cooling rate. The high viscosity at the nose temperature can result from a). a high viscosity at the melting point or liquidus temperatures and b). a viscosity which increases rapidly with falling temperature below the melting point.

Moreover, a large viscosity at the nose temperature is also favored by a high glass-transition temperature, and by a high T_g / T_m ratio. For many good glasses, $T_g / T_m \approx 2/3$

2. No heterogeneous nucleation, due to the presence of even a modest concentration of heterogeneities characterized by small contact can substantially increase the critical cooling rate for glass formation.

3. A large barrier to crystal nucleation. It implies a large crystal-liquid surface energy; and this is turn implies a large entropy of fusion which results to be a good glass.

4. Redistribution of solute required for crystallization. the condition of redistribution of solute directs attention to melt compositions which differ appreciably from those of the respective crystalline phases, including but not restricted to near-eutectic compositions.

2.2 Phosphate glasses

Phosphate glasses have been studied on a laboratory scale during the past 90 years, very few of these materials proved to be a commercial interest. Because of the lack of extensive practical application is primarily related to their poor chemical durability and a tendency to crystallize during processing.

The characteristics of phosphate glasses[7] are large thermal expansion coefficient, low preparation and softening temperatures, low melt viscosity,

chemical compatibility with living bone, and a polymeric structure similar to that inorganic polymers.

2.2.1 Basic chemistry and structure of phosphate glasses

Phosphorus has an electronic configuration of (Ne) ($3s^2$) ($3p^3$). In phosphorus-oxygen bonding, it shows sp^3 hybridization and forms a tetrahedron with four oxygen. A remaining electron promoted to an energetically 3d orbital delocalizes over an oxygen or oxygens via dπ-pπ bonding. Therefore, at least one of the four P-O bonds will show double-bond character. The double-electrons of silicon are ($3s^2$) ($3p^2$). A comparison of the PO_4^- and the SiO_4^- tetrahedra is in Figure 2-4.

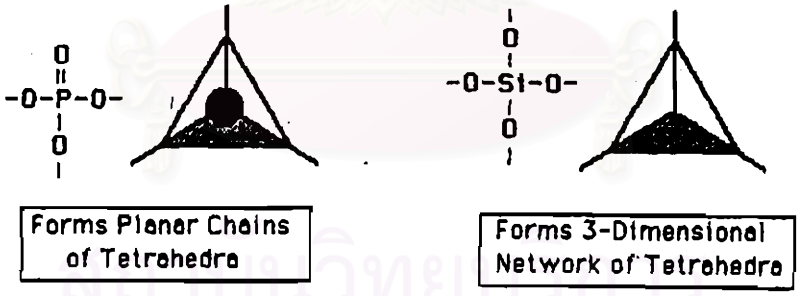

Figure 2-4 Comparison of phosphate and silicate tetrahedra.[8]

The network structure varies with the chemical composition as illustrated in Figure 2-5, there are four types of fundamental structure units constituting these phosphate networks, branching, middle, end, and ortho groups (Figure 2-6). There are three different oxygen types in these

units; a bridge oxygen (P-O_b-P), a non-bridging oxygen (P-O_{nb}), and a double bonded oxygen (P=O_d)

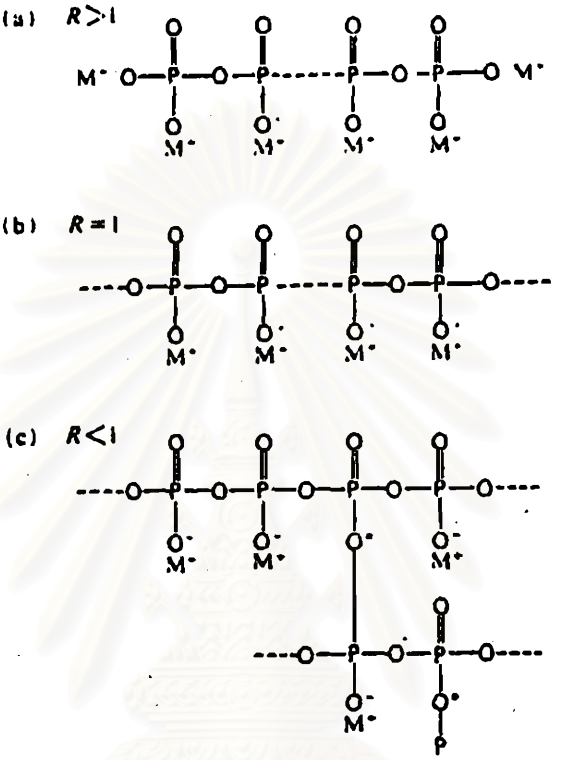

Figure 2-5 Schematic representation of phosphate glass, R = M_2O/P_2O_5 (mole ratio) *denotes branching point.[9]

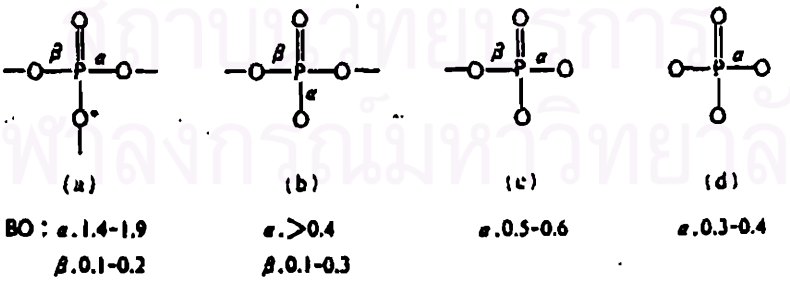

Figure 2-6 Four basic groups constituting the phosphate network. a) branching, b) middle, c) end and d) ortho group. The number of π bonds per σ bond is presented as BO each bond.[9]

In a divalent cation composition, the PO_4^- tetrahedra form planar chains will around the bridging cations, as illustrated in Figure 2-7(a). This 3-D structure is actually that of a "folded-chain", held together by internal divalent cations. And the planar-bound tetrahedra as a regular structure is illustrated in Figure 2-7(b).

(a)

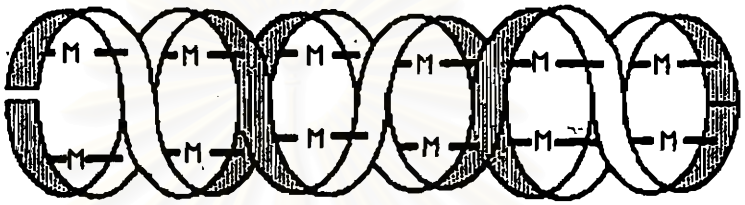

(b)

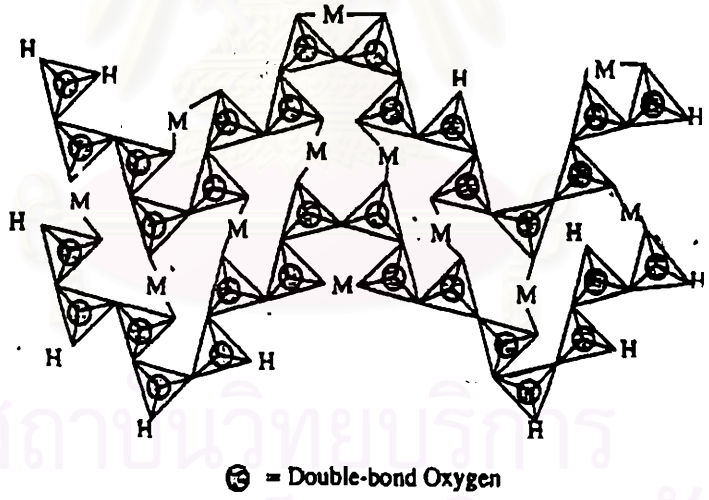

Figure 2-7 a) Planar arrangement of chain structure of tetrahedra in 3-D structure. b) Phosphate chains cross-linked by divalent cation as a regular structure.[8]

Some of the hydroxyl-groups are "terminal", that is they terminate the chain, where as others are "non-terminal", that is they occur

on the sides of the chain. This hydroxyl groups (OH) or non-bridging oxygens almost never occur in silicate glasses whereas it is very common in phosphate-based glasses.

In a phosphate-based structure, can distinguish between bridging and non-bridging sites as illustrated in Figure 2-8 . These are given in terms of the bonds which are formed in a polymeric phosphate chain.

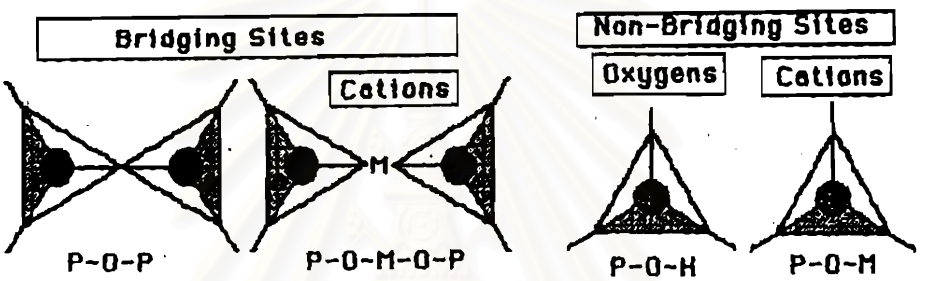

Figure 2-8 Typical sites in a chain structure based on tetrahedra [21]

Two types of bridging sites can occur in these structures, as well as two types of non-bridging sites. However, in a divalent polymerized phosphate glass, it will be shown that the non-bridging cation site does not occur.

One of the characteristic features in the chemical bond P-O is their strong binding force, which is due to the presence of the double bond character. From Table 2-1, this features as the magnitude of force constant of the bond stretching, the P-O bond is the strongest in the coordination tetrahedra of typical glass-forming cations (Si, B, Al, and P), which results in the largest difference in bonding strength between the glass former-oxygen and the counter cation-oxygen. A close similarity is expected between

organic linear polymelts and phosphate glasses of meta or polycomposition. Striking behavior characteristic of the former is that molecular chains are easily oriented by the application of axial tension.

Table 2-1 Force constants an oxygenated tetrahedral and octahedral units[9]

	Force constant for M-O stretching (mdyne / A)[a]
$B(OH)_4^-$	2.1
$AL(OH)_4^-$	2.6
SiO_4^{4-}	4.3
PO_4^{3-}	5.0
LiO_6	0.27
NaO_6	0.18
CaO_6	0.36
BaO_6	0.14

*a) Force constants were evaluated from the vibrational spectroscopic data

2.2.2 Applications for phosphate glasses

Phosphate glasses are being actively studied for application in several areas of technology that include:

1. biocompatible and bioactive glasses for bone and dental implants

2. high-level nuclear waste disposal
3. hermetic glass-to-metal seals
4. glass fibers for strengthening composite materials
5. castable lenses and optical components.

2.3 Viscosity

As to definition: the viscosity (η) is a shearing force (F) which is applied to a liquid by flowing through two parallel surfaces (A) which separate by a given distance (d) at a certain rate (v). It can be expressed as

$$\eta = \frac{Fd}{Av} \qquad (2\text{-}4)$$

The viscosity of a glass is one of the most important properties. It is used to determine the melting conditions which involve in all stirring process and to remove the bubbles during the refining process, working (or forming) and annealing temperature, for nucleation and crystallization and other behaviors of glass; this is illustrated in Table 2-2.

Table 2-2 Illustration in the relation of viscosity, process and behavior.

log η	Name	Process	Behavior
1.5	- -	refining	
3.0	gob temperature (G.T)	melt transferred	predominantly fluid
4.0	--working point (begin of working range)--		
4.22	sinking point (T_E)	FLOAT, SLING	Fluid towards moderately fast deformation, hot fracture occurs
5.0	flow point	PULL, BLOW PRESS, ROLL BEND	upon too fast deformation form memory, but no macroscopic form stability
7.6	littleton point (T_L)		elastic towards macroscopic deformation, i.e. form-state, yet effective relaxation of local stresses
10.0	--transition from working to cool range--		
11.3	dilatometric (T_M)	upper cooling point	macroscopically elastic and brittle
13.0	annealing point (T_g)	glass transition	predominantly elastic and brittle
14.5	strain point	lower cooling point	
19.0		glass at room temp.	elastic and brittle

2.3.1 Temperature dependence of viscosity

The viscosity is proportional to the reciprocal of the temperature as shown in Figure 2-9.

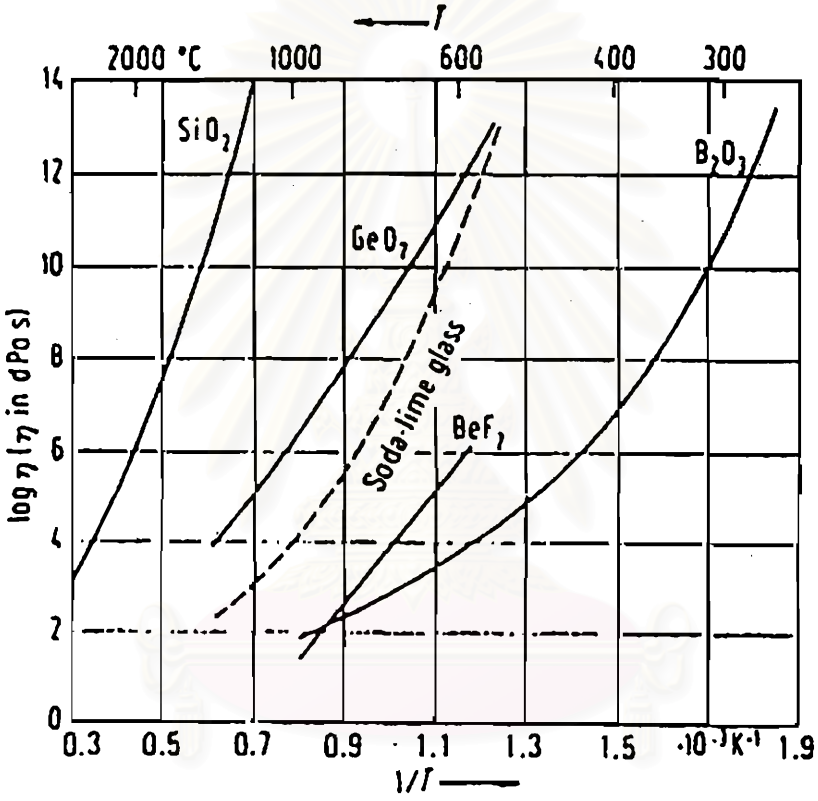

Figure 2-9 Temperature dependence of viscosity of some single-component glass melts.[3]

The relation between the temperature and the viscosity can be described by Vogel-Fulcher-Tamman equation (VFT equation)[3]:

$$L = \log\eta = A + \frac{B}{T - T_o} \qquad (2\text{-}5)$$

where A , B , T_o are VFT constants.

To calculate VFT constants by using three pairs of values , T

$$A = \frac{(L_1 - L_2)(L_3T_3 - L_2T_2) - (L_2 - L_3)(L_2T_2 - L_1T_1)}{(L_1 - L_2)(T_3 - T_2) - (L_2 - L_3)(T_2 - T_1)}$$

$$T_0 = \frac{L_1T_1 - L_2T_2 - A(T_1 - T_2)}{L_1 - L_2}$$

$$B = (T_1 - T_0)(L_1 - A).$$

2.4 Phase separation

The free energy of mixing in the binary system at constant temperature and pressure is expressed as

$$\overline{G} = (1-x)\mu_1 + x\mu_2 \qquad (2\text{-}6)$$

when this equation is separated into standard and rest potentials:

$$\overline{G} = (1-x)\mu_1^o + x\mu_2^o + (1-x)RT\ln a_1 + \ln a_2 \qquad (2\text{-}7)$$

where $\overline{G}$ - the free energy of mixing

x - mole fraction of second component

μ - chemical potential

μ^0 - standard potential of pure component

a - activity

For $x = 0$, $\overline{G} = \mu_1^o$ for $x = 1$, $\overline{G} = \mu_2^o$ (Figure 2-10) the straight line represents the contributions of the standard potentials to $\overline{G}$. In the fact, the contribution of the potentials of real mixture depends on the last two terms in Equation 2-7 which is always negative; so that $\overline{G}$ is convex curve. The tangent in each point is

$$\left[\frac{\partial \overline{G}}{\partial x}\right]_{P,T} = \mu_2 - \mu_1 = \mu_2^o - \mu_1^o + RT\ln\frac{a_2}{a1} \qquad (2\text{-}8)$$

$$= \mu_2^o - \mu_1^o + RT\ln\frac{x}{(1-x)} + RT\ln\frac{f_2}{f_1} \qquad (2\text{-}9)$$

where f - activity coefficient $= a/x,\ a/(1-x)$

Since limits of ln f_2 and ln f_1 are ∞ and 0 for $x \to 0$ and $x \to 1$, respectively. This tangent will use to determine the limit of solution.

In Figure 2-10, to consider $\overline{G}$ curve type I and II. If composition O can separate spontaneously into two phases Q and R; it is true in $\overline{G}$ curve II due to the average energy (point P) is lower than at O, but not in $\overline{G}$ curve I, where the energy at P is higher than at O. This condition can be told that for the region of separation the $\overline{G}$ curve must be convex.

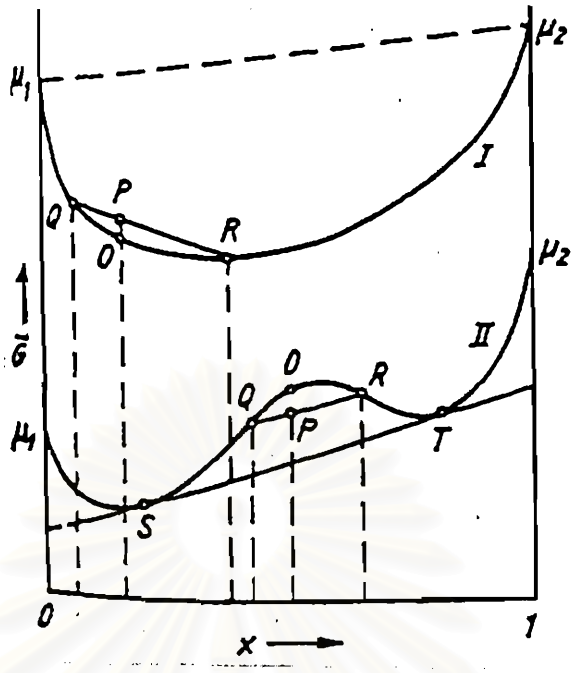

Figure 2-10 The free energy of mixing $\overline{G}$ of a binary system as a function of composition.[10]

2.4.1 The mechanism and kinetics of phase separation.

The mechanism and kinetics of phase separation are illustrated in Figure 2-11. Considering the conditions which use to predict the stability of binary system against composition fluctuations at constant temperature and pressure are as follows:

For stability as well as metastability:

$$(\partial^2 \overline{G} / \partial x^2)_{P,T} > 0$$

For the boundary of stability, the spinodal:

$$(\partial^2 \overline{G} / \partial x^2)_{P,T} = 0$$

For instability:

$$(\partial^2 \overline{G} / \partial x^2)_{P,T} < 0$$

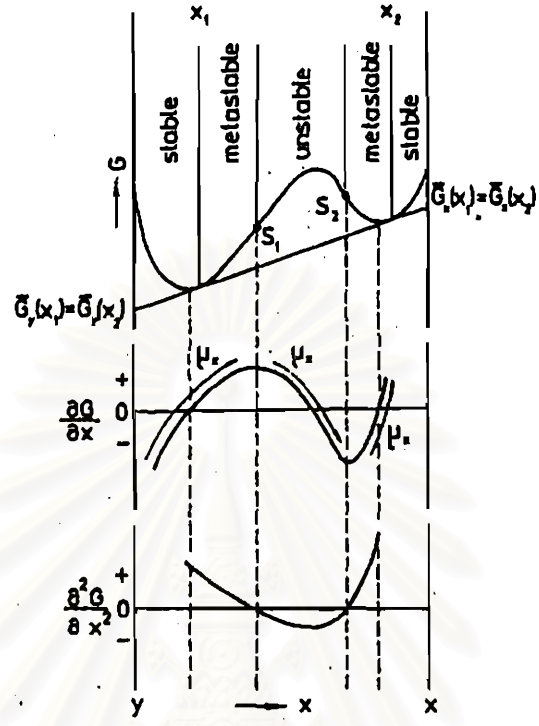

Figure 2-11 Distinguishing between unstable, metastable and stable regions in the $\overline{G} \sim x$ diagram.[11]

2.5 Nucleation process

2.5.1 Homogeneous nucleation

The homogeneous nucleation is described by the classical nucleation theory which was developed by Volmer and by Becker and Doering for vapor → liquid and vapor → solid transformation, and was first applied to solid state reaction by Becker.[12]

The basic assumption of the theory is the formation of a small region of a new phase (β) in the interior of the parent phase (α). In the formation of the new phase region is assumed that it forms homogeneous, its phase boundaries have no formation of stress and the volume of the interfacial energy does not depend on the curvature of the boundary. The free energy change associated with the formation of the region (ΔG_r) can be expressed.

$$\Delta G_r = -\frac{4}{3}\pi r^3 \Delta G_v + 4\pi r^2 \gamma \qquad (2\text{-}10)$$

where γ - the interfacial energy per unit area,

ΔG_v - the bulk free energy per unit volume,

and r - the radius of nuclei.

From Equation 2-10, ΔG_r is the sum of two expressions, one is the bulk free energy per unit volume (ΔG_v) which increases as r^3 and the other is the interfacial energy per unit area (γ) which increases as r^2. From Figure 2-12 when the temperature decreases below the liquidus temperature (T_m), the formation of new phase region can occur. It forms with small radius until it attains a certain critical size (r^*) which is known as a critical radius. The critical radius is associated with a maximum excess free energy (ΔG^*). If $r < r^*$ the new phase is unstable, it can decrease its free energy of the system by dissolution of the new phase. The unstable new phase is known as

embryo or cluster. Whereas when $r > r^*$ the new phase is stable and the further growth becomes spontaneous, so that it is referred to as nuclei.

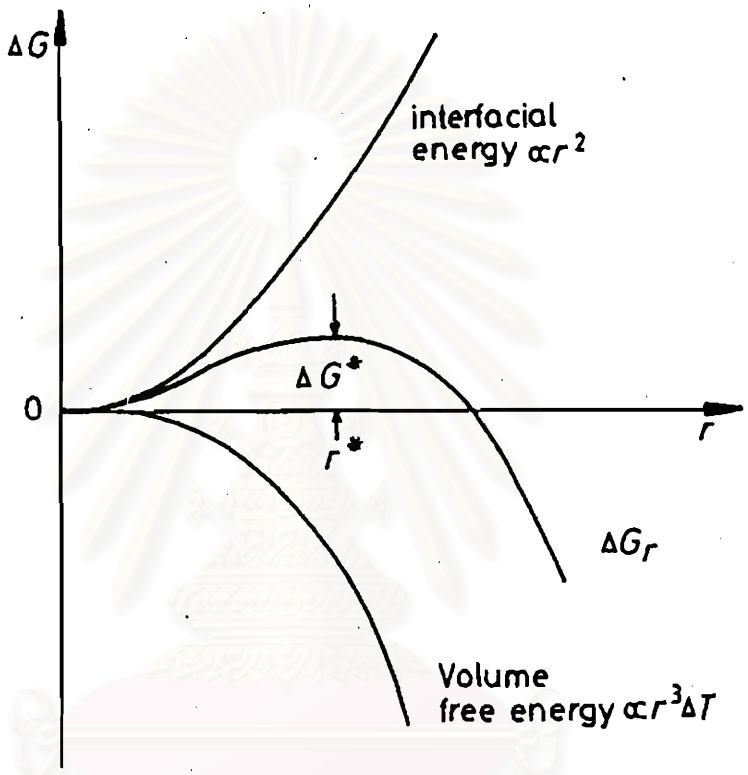

Figure 2-12 The free energy change associated with homogeneous nucleation of a sphere of radius r .[13]

Since $(\partial \Delta G_r / \partial r) = 0$ then $r = r^*$, the critical radius r^* with the maximum excess free energy can be expressed

$$r^* = \frac{2\gamma}{\Delta G_v} \qquad (2\text{-}11)$$

and

$$\Delta G^* = \frac{16\pi\gamma^3}{3(\Delta G_v)^2} \qquad (2\text{-}12)$$

where ΔG^* represents the thermodynamic barrier to homogeneous nucleation.

For an undercooling ΔT, ΔG_v, is given by

$$\Delta G_v = \frac{L_v \Delta T}{T_m} \tag{2-13}$$

where L_v - the latent heat of fusion per unit volume,

thus

$$r^* = \frac{2\gamma T_m}{L_v \Delta T} \tag{2-14}$$

$$\Delta G^* = \frac{16\pi\gamma^3 T_m^2}{3L_v^2} \cdot \frac{1}{(\Delta T)^2} \tag{2-15}$$

From Equations 2-14 and 2-15 can be seen that r^* and ΔG^* decrease with increasing undercooling ΔT.

2.5.2 The homogeneous nucleation rate

The nucleation rate (I_v) is defined as the number of stable nuclei form in unit time in unit volume of parent phase (α). From a pseudo-thermodynamic and kinetic theory, Volume, Becker and Doering[*] and others[25] give the result that I_v is proportional to

$$\exp(-\Delta G^* / kT)$$

And a critical sized embryo can grow into a nucleus by a jump of a few atoms across the interface, this atomic jump is expressed as an activation energy (ΔG_a). So that the rate of interface movement is also proportional to

$$\exp(\Delta G_a / kT).$$

Moreover, the nuclei growth is dependent on the frequency with which atoms adjacent to nucleus. Therefore, the rate at which the critical sized embryo stabilize into nuclei is given by

$$\nu \exp(-\Delta G_a / kT)$$

where ν is the characteristic frequency which is of the order of the Debye frequency and is sometimes written kT/h,

k is Boltzmann's constant ,

and ΔG_a is the activation energy for atomic migration.

If the new and parent phase have the same composition, ΔG_a is identified with the activation energy for the movement of an atom across the interface region. Whereas when the new and parent phase have the different ΔG_a should be the free energy of activation for the diffusion of the slower moving component.

An approximate expression for the nucleation is

$$I_v = N_v \nu \exp(-\Delta G_a / kT) \exp(-\Delta G^* / kT) \qquad (2\text{-}16)$$

$$I_v = N_v \nu \exp(-(\Delta G_a + \Delta G^*) / kT) \qquad (2\text{-}17)$$

where N_v - the number of atoms per unit volume in the parent phase

2.5.3 Heterogeneous nucleation

The heterogeneous nucleation is the formation of the nuclei of a new phase on the surface of an already existing phase boundary. On the other hand, it is described that the formation of the nuclei on an alien crystalline nucleus or a substrate (such as dirt, oxide compound, mold wall and etc.). The difference of the formation between homogeneous and heterogeneous nucleation is shown in Figure 2-13.

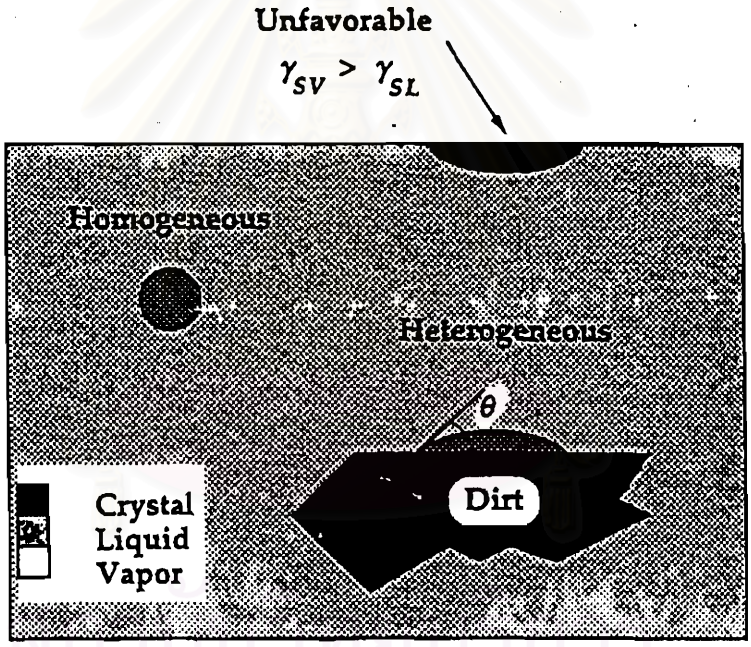

Figure 2-13 Schematic illustration of homogeneous and heterogeneous nucleation [14]

And the formation of heterogeneous nucleation is illustrated in Figure 2-14 (spherical cup model)

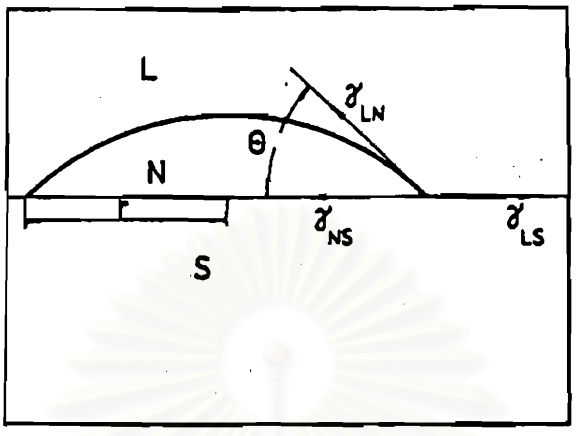

Figure 2-14 Heterogeneous nucleation-spherical cup model L - liquid phase, S - solid phase, N - nucleus-shaped the top of a sphere with radius, θ - wetting angle.[11]

From Figure 2-14 can be expressed an interfacial energy as

$$\gamma_{LS} = \gamma_{NS} + \gamma_{LN}\cos\theta \qquad (2\text{-}18)$$

And the formation of nuclei will be associated with an excess free energy given by

$$\Delta G_{het} = -V_s \Delta G_v + A_{LN}\gamma_{LN} + A_{NS}\gamma_{NS} - A_{NS}\gamma_{LS} \qquad (2\text{-}19)$$

where V_s - the volume of spherical cup

A_{LN}, A_{SN} - the areas of the liquid-nucleus and nucleus-solid interfacial energy

$\gamma_{LN}, \gamma_{NS}, \gamma_{LS}$ - the liquid-nucleus, nucleus-solid and liquid-solid interfacial energies, respectively.

Equation 2-19 can be written in term of the wetting angle (θ) and the cup radius (r) as

$$\Delta G_{het} = \left(-\frac{4}{3}\pi r^3 \Delta G_v + 4\pi r^2 \gamma\right) S(\theta) \qquad (2\text{-}20)$$

where $$S(\theta) = \frac{(2+\cos\theta)(1-\cos\theta)}{4} \qquad (2\text{-}21)$$

And the critical radius (r^*) and the thermodynamic barrier to heterogeneous nucleation (ΔG^*_{het}) can be expressed

$$r^*_{het} = \frac{2\gamma}{\Delta G_v} \qquad (2\text{-}22)$$

and $$\Delta G^*_{het} = \frac{16\pi\gamma^3}{3(\Delta G_v)^2} \cdot S(\theta) \qquad (2\text{-}23)$$

From Equations 2-12 and 2-23 found that the thermodynamic barrier against heterogeneous nucleation (ΔG^*_{het}) is smaller than ΔG^*_{hom} by the shape factor $S(\theta)$ and this is illustrated in Figure 2-15.

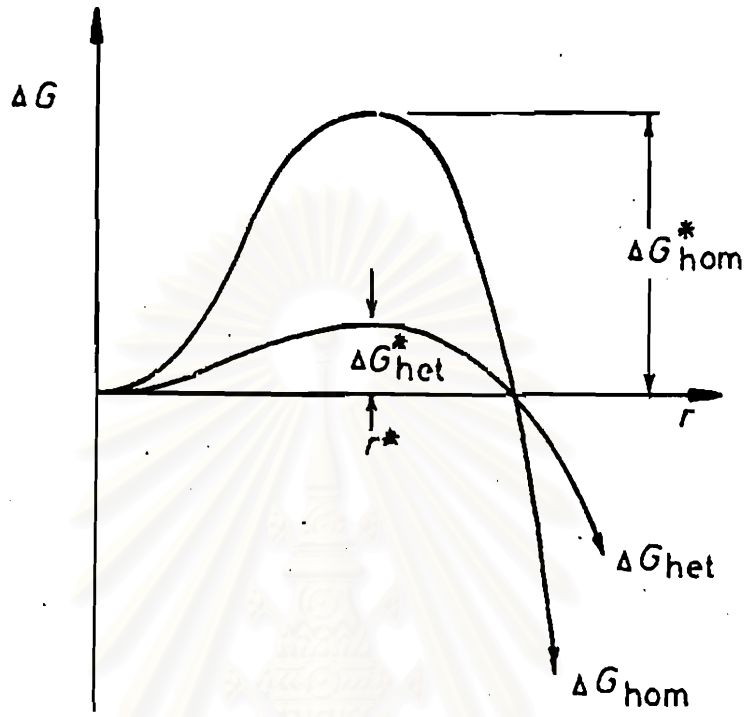

Figure 2-15 The excess free energy of homogeneous and heterogeneous nucleation.[13]

when combining Equation 2-12 and Equation 2-23 give

$$\Delta G^{*}_{het} = \Delta G^{*}_{\text{hom}} \cdot S(\theta).$$

2.5.4 The heterogeneous nucleation rate

The heterogeneous nucleation rate (I_{het}) is similar to the homogeneous nucleation rate, it can be expressed

$$I_{het} = N\nu \exp\left(-(\Delta G_a + \Delta G^{*}_{het})/kT\right) \qquad (2\text{-}24)$$

where ν - the characteristic frequency which is similar to ν in Equation 2-17

N - the number of atoms of the initial phase in contact with the surface of the heterogeneity per unit volume of the initial phase.

2.6 Crystal growth

The crystallization of the new phase will proceed after a stable nuclei has been formed in the parent phase. The growth rate of the new phase is controlled as follows:

a) by the rate of heat transfer at the phase boundary

b) by the rate of transfer of structural unit

c) by the rate of the reaction in which the structural units are incorporated into the crystal lattice.

In glass-forming systems, the crystal growth is mostly controlled by molecular transport or by reactions at the interface between the crystal and melt. The theoretical description of the crystallization process is based on a different assumption concerning the interface and the nature of the site on the interface where atoms (molecules) are incorporated or removed.

Jackson[15] found that, the nature of the interface has been related to a bulk thermodynamic property, the entropy of fusion. For crystallization processes involving low entropy changes ($\Delta S < 2R$), the interface will be

crystallographically rough on atomic scale and the growth anisotropy will be small. The kinetics of crystallization is the normal growth model. In contrast, for crystallization involving high entropy changes ($\Delta S > 4R$), materials have crystallographically smooth interface for close packed planes and the growth anisotropy will be large. In this case, the kinetics of crystallization is the models of two-dimensional nucleation or screw dislocation.

2.6.1 The models of crystal growth

Three standard models used to describe crystal growth and their respective predictions of kinetic behavior are :

1. Normal (Rough surface) growth model:

The normal growth model is described by Wilson and Frenkel.[16] It is assumed that the atoms (molecules) can be added or removed at any sites on the crystal surface and the fraction of active sites (f) at which incorporation of atoms (molecules) occurs equals one with respect to overall number of sites on the surface. In this typically model, the growth occurs on the interface as rough on an atomic scale. The growth rate is expressed:

$$U = \nu a_0 \left[1 - \exp(-\Delta G / kT)\right] \qquad (2\text{-}25)$$

where
$$\nu = \frac{kT}{3\pi a_0^3 \eta} \qquad (2\text{-}26)$$

where U - the growth rate per unit area of the interface.

ν - frequency factor for transport at the crystal-liquid interface.

a_0 - the distance advanced by the interface in a unit kinetic process, approximately a molecular diameter,

ΔG - the free-energy change accompanying crystallization

η - viscosity

At equilibrium, if $\Delta G << kT$, the growth rate will be linear in time and is proportional to the undercooling ($U \sim \Delta T$). In the other hand when $\Delta G >> kT$. The growth rate is limited which can expressed in term $U \rightarrow \nu a_0$. This condition is illustrated in Figure 2-16.

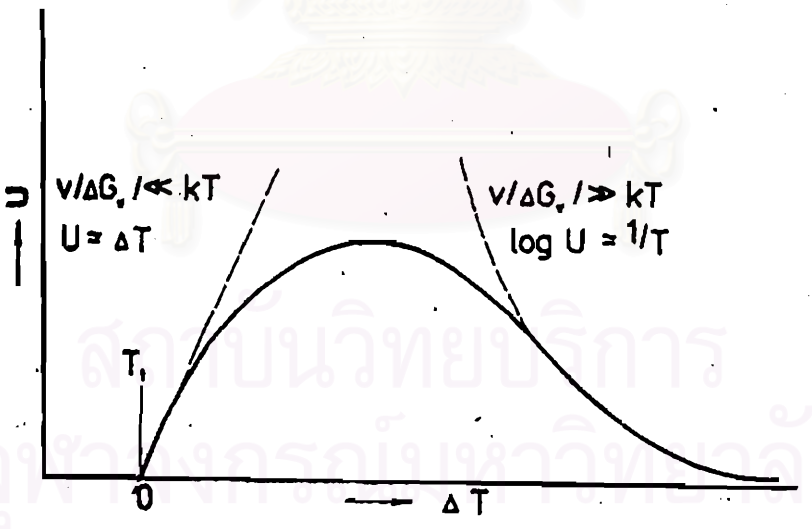

Figure 2-16 Dependence of the growth rate U on the undercooling ΔT; T_m - melting point [11]

2. Screw dislocation growth model

In this typically model, the crystal growth proceeds across the interface and the interface is as smooth but imperfect on an atomic scale. Hillig and Turnball[17] described this typically growth is continuous crystal growth on a crystallographically smooth surface can also be achieved by spiral growth. The formation of a screw dislocation at the interface will occur the incorporation of structural unit by a new permanent formation and a suitable sites at the interface is the crystal surface which forms incomplete. The fraction of sites is approximately

$$f \approx \frac{\Delta T}{2\pi T_m} \tag{2-27}$$

and growth rate $$U = f\nu a_0\left[1-\exp(-\Delta G / kT)\right] \tag{2-28}$$

where f - the fraction of preferred growth sites (at the dislocation ledges) on the interface

T_m - melting or liquidus temperature

At equilibrium, if undercooling changes small, the growth rate of a screw dislocation is proportional to the square of the undercooling, $U \sim (\Delta T)^2$.

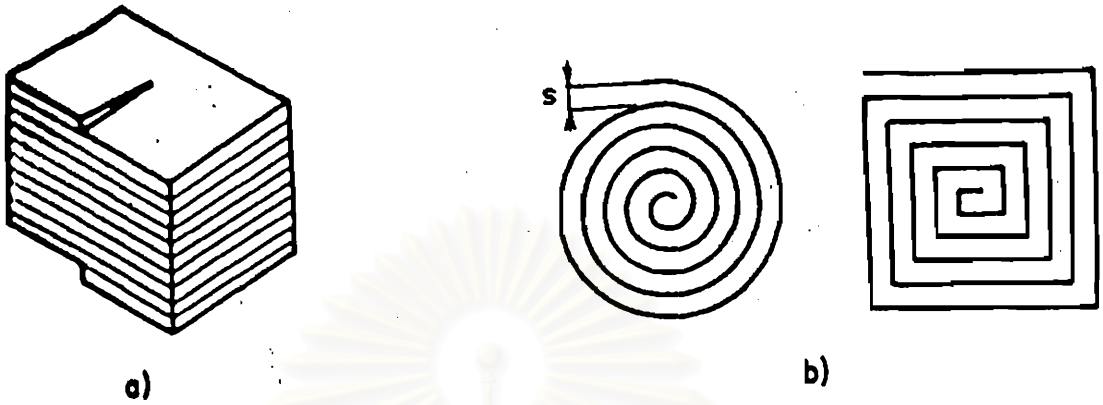

Figure 2-17 Schematic depiction of the mechanism of spiral growth a) a screw dislocation through the crystallographic plane, b) two types of spiral growth with step widths.[11]

3. Surface nucleation growth model

Similar to the screw dislocation growth model, the crystal growth proceeds across the interface. The interface must be as smooth and perfect on an atomic scale. In this model Hilling described the surface is already full, then the formation of a new surface requires the formation of a new site for further growth. Thus the growth can be attained on a crystallographically smooth surface by two-dimensional nucleation, which this growth is called the surface nucleation growth model. According to this model, the rate of crystal growth depends on the frequency of formation and distribution of two-dimensional nuclei at the interface. The growth rate is expressed:

$$U = A\nu \exp\left(\frac{-B}{T\Delta T}\right) \qquad (2\text{-}29)$$

where the exponential constant B is proportional to the square of the edge surface energy of a two-dimensional nucleus.

From three models of the crystal growth can decribe the mechanism of crystal growth at the phase boundary in Figure 2-18.

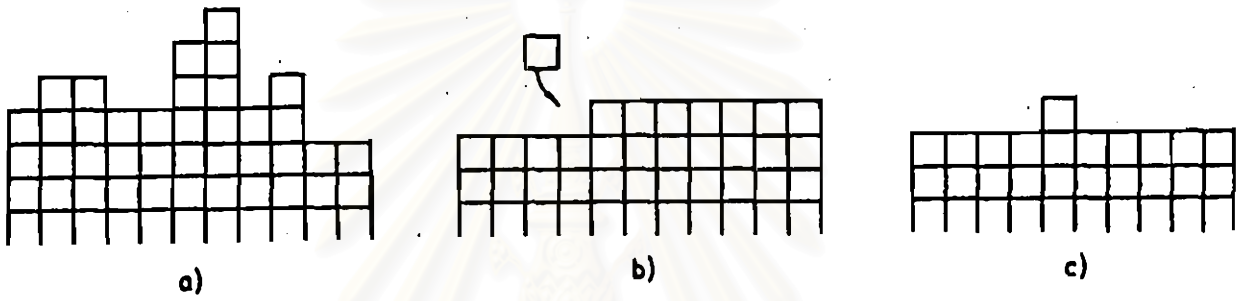

Figure 2-18 Schematic depicting of the mechanism of crystal growth at the phase boundary. a) noncrystallographic phase boundary, i.e. rough compared to the structural unit, b) energetically favorable addition of structural units, c) formation of nuclei on a crystallographically smooth phase boundary of two - dimensional nucleation.[11]

2.7 Phase transformation involving nucleation and growth

2.7.1 Isothermal transformation conditions.

Phase transformation of nucleation and growth such as glass crystallization can be described by Johnson-Mehl-Avrami (JMA) equation[18], which is followed as:

$$x(t) = 1 - \exp[-kt^n] \qquad (2\text{-}30)$$

where $x(t)$ - the volume fraction crystallized after time t ,

n - the mechanism constant (Table 2-3)

k - the reaction rate constant and is expressed by Arrhenius equation:

$$k = \nu \exp -[E / RT] \qquad (2\text{-}31)$$

where ν - the frequency factor

E - the activation energy

R - the gas constant

T - the temperature in (K)

The isothermal transformation rate, $\frac{dx(t)}{dt}$, can be determined from Equation 2-30 by differentiation with respect to time.

$$\frac{dx(t)}{dt} = knt^{n-1} \exp[-kt^n] \qquad (2\text{-}32)$$

Because of the explicit reaction between x and t given by Equations 2-30 and 2-32 can be rewritten equivalently as:

$$\frac{dx}{dt} = nk^{1/n}(1-x)\left[\ln\left(\frac{1}{1-x}\right)\right]^{(n-1)/n} \qquad (2\text{-}33)$$

Table 2-3 A summary of n found under various transformation conditions. [19]

Values of n in kinetic law $x(t) = 1 - \exp[-kt^n]$

I. Polymorphic changes, discontinuous precipitation's, eutectoid reactions, interface controlled growth, etc..

Transformation conditions	n
Increasing nucleation rate	>4
Constant nucleation rate	4
Decreasing nucleation rate	3-4
Zero nucleation rate (saturation of point sites)	3
Grain edge nucleation after saturation	2
Grain boundary nucleateion after saturation	1

II. Diffusion controlled growth

Transformation conditions	n
All shapes growing from small dimension, increasing nucleation rate	>2 ½
All shapes growing from small dimensions, constant nucleation rate	2 ½
All shapes growing from small dimensions, decreasing nucleation rate	1 ½ - 2 ½
All shapes growing from small dimensions, zero nucleation rate	1 ½
Growth of particles of appreciable initial volume	1-1½
Needles and plates of finite long dimensions, small in comparison with their separation	1
Thickening of long cylinders (needles) e.q., after complete end impingement	1
Thickening of very large plates e.q., after complete edge impingement,	½
Precipitation on dislocations (very early stager)	~⅔

From Equation 2-33 is sometimes referred to as the Johnson-Mehl-Avrami transformation rate equation, which indicates that under isothermal conditions there is a unique relationship between the fraction transformation (x), and the transformation rate, $\frac{dx(t)}{dt}$.

Equation 2-30 can be rearranged into the equation of a line by taking the logarithm it is expressed as

$$\ln(1-x) = -kt^n \qquad (2\text{-}34)$$

$$\ln[-\ln(1-x)] = \ln k + \ln t \qquad (2\text{-}35)$$

At a given temperature; from an isothermal DSC/DTA curve the fraction crystallized (x) will be determined as illustrated in Figure 2-19 (a). Value of n and k are determined using Equation 2-35 by plot $\ln[-\ln(1-x)]$ vs $\ln t$ as illustrated in Figure 2-19(b), the slope of the line in Equation 2-35 is the n value and the y - intercept is the $\ln k$ value. The last, the activation energy of crystallization E and the frequency factor ν and determined by taking the logarithm of Equation 2-31; the logarithmic form of Equation 2-31 is

$$\ln k = \ln \nu = E / RT \qquad (2\text{-}36)$$

Then plot $\ln k$ vs $/T$ as illustrated in Figure 2-19(c), the slope of the line is the E - value .

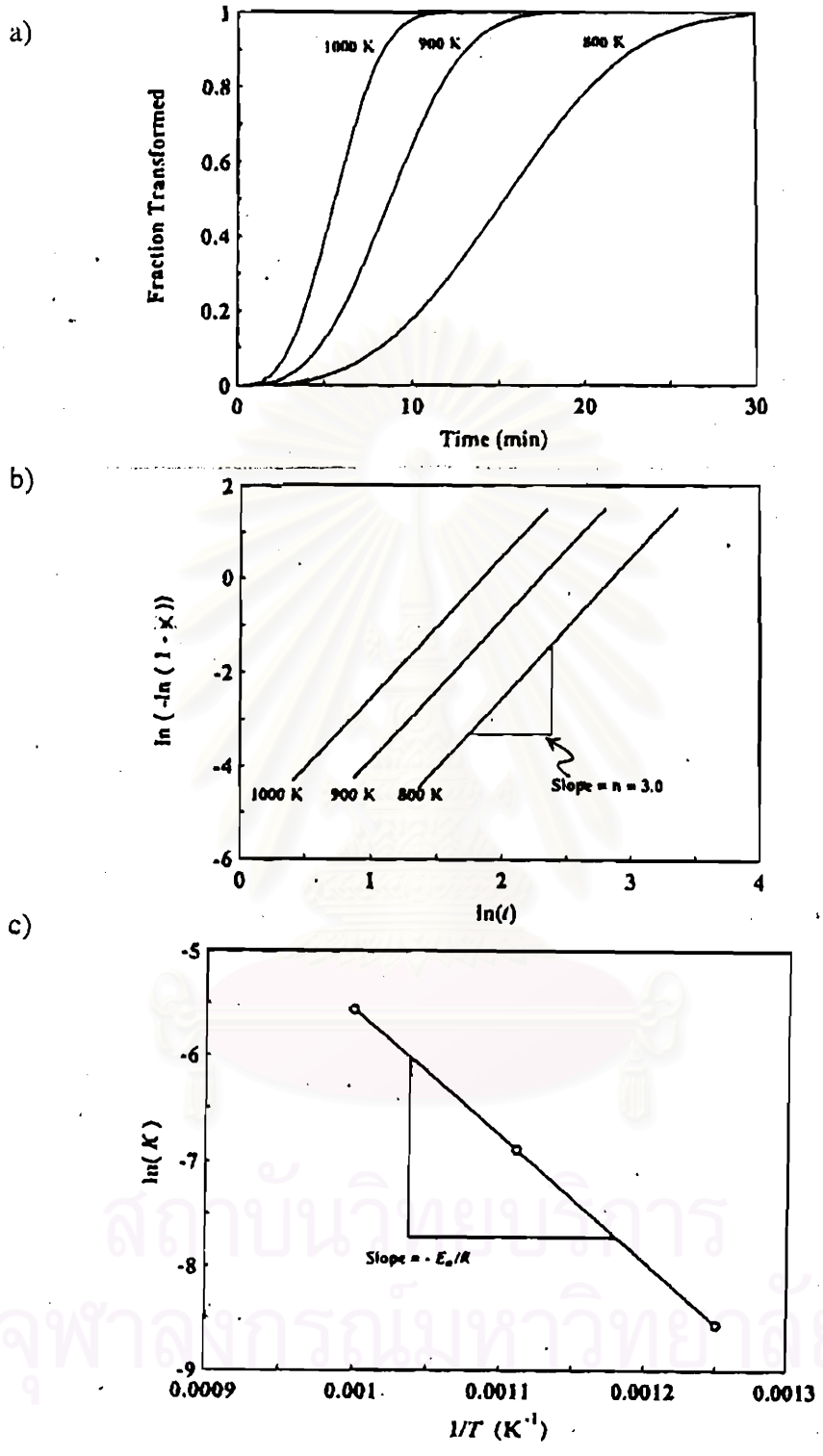

Figure 2-19 a). the plot of fraction crystallized (x) after time t, b). A JMA plot follows by Equation 2-35, c). Arrhenius plot to determine the activation energy of crystallization.[31]

2.7.2 Nonisothermal transformation condition

The method of Augis and Bennett[20] is used to describe in this condition. In a nonisothermal (dynamic) DTA experiment, the temperature is change linearly with time at a given rate , i.e.

$$T = T_0 + \alpha t \tag{2-37}$$

where T_0 - the initial temperature (in K)

T - the temperature after time (in K)

From Avrami law for the fraction transformed:

$$x = 1 - \exp\left[-(kt)^n\right] \tag{2-38}$$

Because of Equation 2-37 the rate constant varies with time and kt is no longer linear in t but a more complicated function such as:

$$kt = u = \nu t \exp\left[-E / R(T_0 + \alpha t)\right] \tag{2-39}$$

and Equation 2-38 becomes

$$x = 1 - \exp(-u)^n \tag{2-40}$$

The second derivation of x with time ($\ddot{x}$) is

$$\ddot{x} = \left[\ddot{u}u - \dot{u}^2\left(nu^n - n + 1\right)\right]nu^{n-2}(1-x) = 0 \qquad (2\text{-}41)$$

where $\ddot{x} = d^2x/dt^2$, $\ddot{u} = d^2u/dt^2$, $\dot{u} = du/dt$

Assuming that the maximum rate of reaction agrees with the DTA peak, its position is given by

$$\ddot{u}u - \dot{u}^2\left(nu^n - n + 1\right) = 0 \qquad (2\text{-}42)$$

Since there is $T = T_0 + \alpha t$ and simplifying

$$\dot{u} = \nu \exp\left(-\frac{E}{RT}\right) + \frac{\nu t E\alpha}{RT^2}\exp\left(\frac{-E}{RT}\right)$$

or $$\dot{u} = \frac{u}{t} + au = u\left[\frac{1}{t} + a\right]$$

where $$a = \frac{E\alpha}{RT^2}$$

and $$\ddot{u} = \frac{\dot{u}}{t} - \frac{u}{t^2} + a\dot{u}$$

or $$\ddot{u} = \dot{u}\left(\frac{1}{t} + a\right) - \frac{u}{t^2} = u\left[\left(\frac{1}{t} + a\right)^2 - \frac{1}{t^2}\right]$$

Equation 2-42 becomes

$$u^2 = \left[\left(\frac{1}{t}+a\right)^2 - \frac{1}{t^2}\right] - u^2\left[\left(\frac{1}{t}+a\right)^2\right]\left(mu^n - n + 1\right) = 0$$

and is satisfied if

$$mu^n - n + 1 = 1 - \frac{1}{(1-at)^2} \qquad (2\text{-}43)$$

Putting back the original expression for u, i.e., Equation 2-39 we have

$$\nu^n \exp\left[\ln\frac{E}{RT_p}\right] = \left[\frac{T_p - T_0}{\alpha}\right]^{-n}\left[1 - \left(\frac{1}{n\left(1+\left(\frac{E}{R}\cdot\frac{(T_p - T_0)}{T_p^2}\right)\right)}\right)\right] \qquad (2\text{-}44)$$

where T_p corresponds to the temperature of the maximum of the DTA curve.

Equation 2-44 can be solved graphically for E/R if ν is assumed or known. Thus, the study of solid-state reactions by DTA without the prior knowledge of the frequency factor. DTA has been used to investigate kinetics of reactions by the Kissinger method. The fundamental expression of Kissinger 's method is:

$$\nu \exp\left(\frac{-E}{RT_p}\right) = \frac{E\alpha}{RT_p^2} \qquad (2\text{-}45)$$

For most solid-state reactions can observe that $E > 10$ kcal/mol and $T_p < 3000$ K

So $$\frac{E}{R}\cdot\frac{(T_p - T_0)}{T_p^2} >> 1$$

Therefore, Equation 2-41 becomes:

$$\nu^n \exp\left(\frac{nE}{RT_p}\right) \approx \left(\frac{(T_p - T_0)}{\alpha}\right)^{-n} \quad (2\text{-}46)$$

Equation 2-46 is assumed $n = 1$, so that

$$\nu \exp\left(\frac{E}{RT_p}\right) \approx \left(\frac{(T_p - T_0)}{\alpha}\right)^{-1} \quad (2\text{-}47)$$

The logarithmic form of Equation 2-47 is

$$\ln\frac{\alpha}{(T_p - T_0)} = \ln\nu - \frac{E}{RT_p} \quad (2\text{-}48)$$

Then plot $\ln\frac{\alpha}{(T_p - T_0)}$ versus $\frac{1}{T_p}$, so the slope of the line is $\frac{-E}{R}$ and the y - intercept is $\ln\nu$ (Figure 2-20)

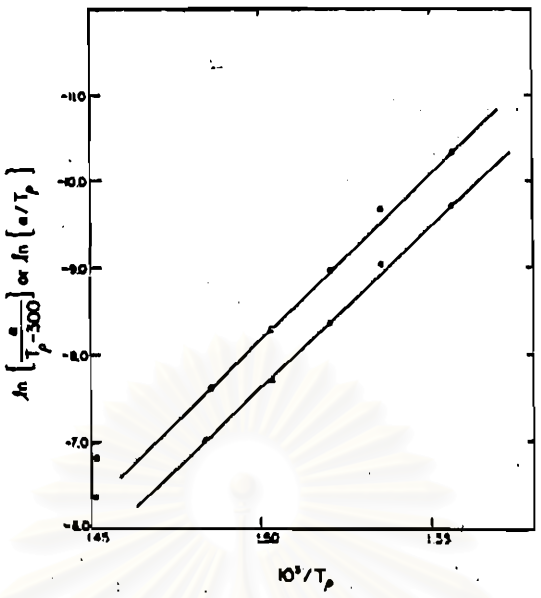

Figure 2-20 The plot of $\ln\dfrac{\alpha}{(T_p - T_0)}$ versus $\dfrac{1}{T_p}$. [21]

Augis and Bennett[20] pointed out that reactions with the same E but different n will show a crystallization peak at the same temperature. The value of n determines the shape of the peak; the higher the value of n, the narrower the peak. They gave the following expression for estimating the value of n :

$$n = \frac{2.5}{\Delta T_{FWHM}} \cdot \frac{T_p^2}{E/R} \qquad (2\text{-}48)$$

where ΔT_{FWHM} is the width of the crystallization peak at half maximum.

2.8 Literature Survey

In 1963, Cormia et al.[22] studied the kinetics of melting and crystallization of phosphorus pentoxide by the use of a microscopic technique. It was found that the superheating of about 50 °C above the melting temperature (580 °C) was possible. The melting was heterogeneous and begins only at free surface or grain boundaries but never within a crystal, similar to a silicate melting. Both melting and crystallization depended on temperature, time crystal direction, morphology and thermal history.

In 1973, Abe[23] studied the kinetics of crystallization of calcium metaphosphate glass by using high temperature microscopy and high temperature X-ray diffraction techniques. It was found that the activation energy of nucleation of β-calcium metaphosphate which was calculated by Arrhenius plots, was 155 kcal/mol. The activation energys of crystallization was 188 kcal/mol. And by applying the JMA equation, the crystal growth was three-dimensional growth.

In 1976, Abe et al.[24] reported that the crystallization of $Ca(PO_3)_2$ glass could occur below the glass transition temperature. This experiment showed that at the extrapolated heating rate of zero, the glass transition temperature (T_g) was 490 °C, while the glass the hemispherulite formed at 420 °C ($< T_g$) and the spherulite and/or hemispherulite formed at 600 °C ($> T_g$).

In 1982, Abe et al.[25] prepared high strength $Ca(PO_3)_2$ glass-ceramics by unidirectional crystallization. The unidirectionally crystallized

glass showed extremely high bending strength (about 500 to 600 MN/m^2) and the fracture surface revealed a typical fiber-reinforced-composite structure.

In 1984, Abe et al.[26] prepared calcium phosphate glass-ceramic crown by lost-wax technique. This crown was developed for dentistry. The process was to cast the glass into the shape of the crown by the lost-wax technique and subsequently heat treated to convert it into the glass-ceramic. The prepared crown exhibited excellent mechanical strength, its fine structure was similar to that of the enamel of a natural tooth and its hardness was near that of enamel.

In 1986, Watanabe et al.[27] studied periodic accumulation of voids in calcium phosphate glass-ceramics. They found that after the crystallization of calcium phosphate glass a pattern of stripes like the rings of a tree was observed in the glass-ceramic. The pattern of stripes, formed only from a particular glass composition and under specific crystallization conditions, was made up of voids resulting from a difference in density between the original glass and the resulting glass-ceramics. The size and distribution pattern of these voids had to be controlled to achieve maximum mechanical properties.

In 1988, Matsubara et al.[28] studied the structure of binary phosphate glasses with MgO, ZnO, and CaO by X-ray diffraction. The X-ray diffraction profiles of magnesium, zinc, and calcium phosphate glasses had been measured and the pair function distributions (PFDs) were calculated. Using the pair function method, distance and coordination numbers for the pairs of P-O, O-O, and M-O (M = Mg, Zn, and Ca) were determined a

fundamental unit of the structure in these phosphate glasses was confirmed to be a PO_4 tetrahedron. It was found that in the calcium phosphate glass the PO_4 tetrahedral form long chains and almost all Ca^{2+} were surrounded by 6 oxygen which agreeed with the structure model by other workers.

In 1991, Chin-Wang Huang et al.[29] studied the kinetics of apatite (CaO/P_2O_5) glass ceramics, containing Al_2O_3. The observation of devitrification phenomenon and crystallization kinetics of CaO/P_2O_5, containing Al_2O_3 were investigated by using non-isothermal technique and they found that CaO/P_2O_5, containing Al_2O_3 glass trended to crystallize from surface towards the inside and the major phases were β-CaP_2O_6 , β-$Ca_2P_2O_7$, and δ-CaP_2O_6.

In 1992, Nan et al.[30] studied the crystallization behavior of CaO-P_2O_5 glass with TiO_2 , SiO_2 , and Al_2O_3 additions. They found that TiO_2 about 4 mol% was an effective nucleating agent for CaO- P_2O_5 glass which also contains substantial SiO_2 and Al_2O_3 additions. Powder of this composition crystallized rapidly to β-$Ca_2P_2O_7$, whereas bulk glass crystallized from diphasic nuclei consisting of a central cubic Ca-P-Ti-Si-Al oxide phase surrounded by impure dendrites. Metastable calcium phosphate grows on the $AlPO_4$ dendrites and later transforms to β-$Ca_2P_2O_7$.

In a part of phosphate glass fiber, the research work was as follows:

In 1955, Goldstein and David[31] studied glass fibers with oriented chain molecules. They prepared by melting the material on platinum loops and drew the loops apart very slowly until the glass was viscous enough for

its resistance to flow to be felt. They found that under drawing conditions indicated by the theory of viscoelastic properties of high polymers, fibers of sodium metaphosphate glass had been prepared that showed birefringence and gave X-ray diffraction patterns similar to those of organic fibers with oriented chain molecules. Under analogous treatment sodium metasilicate failed to such effects.

In 1963, Milberg and Daly[32] prepared $NaPO_3$ glass fibers which were similar to Goldstein's preparation and studied structure of oriented sodium metaphosphate glass fibers. The results indicated that $NaPO_3$ fibers were made up of long chains of PO_4 tetrahedra, and that the axes of these chains had a strong preference for lying along the fiber axis direction.

In 1973, Miller et al.[33] prepared $NaPO_3$ glass fibers and studied vibrational spectrum of molecular orientation in vitreous fibers. The vitreous fibers was demonstrated by laser Raman and infrared reflectance. They found that preferential orientation of polymeric chain respects to the principle axis in completely noncrystalline.

In 1986, Stockhorst and Brueckner[34] prepared $25Li_2O{\cdot}25\ Na_2O{\cdot}50\ P_2O_5$ and $25CaO{\cdot}25BaO{\cdot}50P_2O_5$ glass fiber and studied behaviors of glass fibers. They found that the structure of meta-phosphate glass fibers was influenced mainly by three parameters: nozzle temperature, cooling rate (thermal prehistory) and drawing stress (mechanical prehistory).